

Quantum Noise in the Parametric Oscillator: From Squeezed States to Coherent-State Superpositions

M. Wolinsky and H. J. Carmichael

Department of Physics, University of Arkansas, Fayetteville, Arkansas 72701

(Received 1 February 1988)

We compare the nonclassical states of light produced by a parametric oscillator for quantum noise of different strengths. Increasing noise strength brings a transition from a slightly perturbed classical state showing squeezing to a superposition of coherent states. We use the positive- P representation to illustrate the roles of quantum noise, quantum coherence, nonlinearity, and dissipation in this simple quantum dynamical system.

PACS numbers: 42.50.Dv, 03.65.Bz, 42.50.Kb, 42.65.Ky

Recent experiments producing squeezed light have added a new nonclassical light source to the few available, thereby rekindling interest in nonclassical states of the electromagnetic field. The degenerate parametric oscillator has played a central role in studies of squeezing; its Hamiltonian is intimately related to the infinitesimal generator of squeezed states. Moreover, it enjoys the distinction of having produced the greatest amount of squeezing observed to date.^{1,2}

In a sense, however, parametric oscillators that produce squeezed light are almost classical; they are classical systems driven by a *very small* quantum noise — “small” in the sense (mathematically) that a linearized treatment of the quantum dynamics is valid, and (physically) that many photons are needed to probe the system’s nonlinearity. In this Letter we present a treatment of the degenerate parametric oscillator valid for quantum noise of arbitrary strength. Our approach is based upon the positive- P representation. We find an analytic solution for the steady-state positive- P function. This solution is a function of two phase-space variables; one variable is the “classical” field amplitude of semiclassical nonlinear optics; the other is a “nonclassical” variable needed to represent *superpositions* of coherent states. When the positive- P function is plotted in three dimensions the role of the nonclassical variable can be clearly visualized. Distinct pictures emerge for the limiting regimes of essentially classical behavior and predominantly quantum behavior. This distinction is drawn from the novel feature that the quantum dynamics is naturally confined to a *bounded* manifold in phase space; the extent to which the noise has sufficient strength to probe the boundary provides a measure of the deviation from a classical state. This bounded manifold provides a beautiful illustration of the subtle way in which recently reported anomalies in stochastic simulations based on the positive- P representation may be resolved.³

The degenerate parametric oscillator is modeled by two quantized field modes, with frequencies ω and 2ω , interacting via a $\chi^{(2)}$ susceptibility inside an optical cavity. Both modes are resonant with the cavity and experi-

ence linear loss. The cavity is excited by a classical pump field with frequency 2ω . The microscopic Hamiltonian takes the form

$$H = i\hbar \frac{1}{2} \bar{g} (\hat{a}^\dagger \hat{b} - \hat{a}^2 \hat{b}^\dagger) + i\hbar \mathcal{E} (\hat{b}^\dagger - \hat{b}) + H_{\text{loss}}, \quad (1)$$

where \hat{a} and \hat{a}^\dagger , and \hat{b} and \hat{b}^\dagger , are annihilation and creation operators in the interaction picture; \bar{g} is the mode-mode coupling constant; \mathcal{E} is the intracavity pump-field amplitude; and H_{loss} describes losses in the nonlinear crystal and at the cavity mirrors.

This nonlinear quantum-mechanical problem can be mapped by an appropriate phase-space representation into a classical stochastic process. The familiar Glauber-Sudarshan P representation gives a Fokker-Planck equation without positive-definite diffusion. This difficulty can be overcome with the positive- P representation. With mode \hat{b} adiabatically eliminated we obtain the following set of Ito stochastic differential equations for the complex amplitude⁴ of mode \hat{a} :

$$\begin{aligned} d\alpha &= [-\alpha - \alpha_* (\lambda - \alpha^2)] d\tau + g(\lambda - \alpha^2)^{1/2} dW_1, \\ d\alpha_* &= [-\alpha_* + \alpha (\lambda - \alpha_*^2)] d\tau + g(\lambda - \alpha_*^2)^{1/2} dW_2, \end{aligned} \quad (2)$$

where dW_1 and dW_2 are independent Wiener increments, τ is measured in cavity lifetimes (γ_a^{-1}), $g = \bar{g}/(2\gamma_a\gamma_b)^{1/2}$, and λ is a dimensionless measure of the pump-field amplitude scaled to give the threshold condition $\lambda = 1$; γ_a and γ_b are decay rates for the cavity fields. The complex variables α and α_* are associated with operators \hat{a} and \hat{a}^\dagger , respectively. Stochastic averages of α and α_* give the operator averages $g\langle\hat{a}\rangle$ and $g\langle\hat{a}^\dagger\rangle$. In the Glauber-Sudarshan representation α and α_* are complex conjugates. In the positive- P representation they are not, although they must be so in the mean. More generally, normally ordered averages of quantum operators are calculated from the positive- P function, $P(\alpha, \alpha_*)$, with

$$\langle\hat{a}^{\dagger n} \hat{a}^m\rangle = g^{-(n+m)} \int d^2\alpha \int d^2\alpha_* \alpha_*^n \alpha^m P(\alpha, \alpha_*). \quad (3)$$

Equations (2) describe trajectories in a four-dimen-

sional phase space. The region of phase space satisfying the conjugacy condition $\alpha_* = \alpha^*$ is designated the *classical* subspace, since it is within this subspace that the equations of semiclassical nonlinear optics evolve. Two extra *nonclassical* dimensions are required by the quantum noise. If we neglect dW_1 and dW_2 , Eqs. (2) have the stable steady-state solution $\alpha = \alpha_* = 0$ below threshold ($\lambda < 1$); above threshold ($\lambda > 1$) this becomes unstable and two new stable solutions $\alpha = \alpha_* = \pm (\lambda - 1)^{1/2}$ appear. These are the steady states of the classical parametric oscillator. In the full phase space there are additional steady states which do not satisfy the conjugacy condition: two steady states $\alpha = \alpha_* = \pm i(1 - \lambda)^{1/2}$ below threshold, and two steady states $\alpha = -\alpha_* = \pm (\lambda + 1)^{1/2}$ both below and above threshold. These additional steady states evidence a major reorganization of the deterministic nonlinear dynamics in the expanded phase space. This reorganization can lead to anomalous behavior (unstable trajectories) in numerical simulations of Eqs. (2) for large quantum noise ($g \gtrsim 1$)³. However, respect for a reflecting boundary condition embedded in the equations removes this difficulty; moreover, this observation leads to an analytic solution for the steady-state positive- P function.

Consider the bounded manifold $\alpha = x$, $\alpha_* = y$, with x and y both real and $|x|, |y| \leq \sqrt{\lambda}$. We denote this manifold by $\Lambda(x, y)$. Stochastic trajectories starting within this manifold must at first preserve α and α_* as real quantities, since λ, g, dW_1 , and dW_2 are all real, and the arguments of the square roots in Eqs. (2) are both positive. It is a small step to conclude that, in fact, α and α_* remain real, and within $\Lambda(x, y)$ for all time. To escape from this manifold one of the square roots must obtain a negative argument. The boundary of $\Lambda(x, y)$ is defined by the condition that one or the other square root (noise term) vanishes. Since the stochastic trajectories

are strictly continuous functions of time, this boundary must be crossed; it cannot be jumped. But noise transverse to the boundary vanishes, and the deterministic flow transverse to the boundary is directed inwards, as illustrated in Fig. 1. A trajectory reaching the boundary can only move along the boundary under the influence of the nonvanishing noise term, or return to the interior of $\Lambda(x, y)$ under the deterministic flow. Thus, trajectories entering $\Lambda(x, y)$ are confined within it. The vacuum state (the natural initial condition), as well as all stable steady states of the deterministic equations, is contained within $\Lambda(x, y)$. The unstable steady states and those regions of phase space which can lead to unstable numerical trajectories lie outside. Of course, unless directed not to do so, trajectories generated by numerical algorithms, taking finite steps, can jump the boundary; this opens the possibility for the instabilities seen in naive simulations of Eqs. (2).

The manifold $\Lambda(x, y)$ is alternatively denoted by $\Lambda(u, v)$, with $u = \frac{1}{2}(x + y)$, and $v = \frac{1}{2}(x - y)$. The line $v = 0$ is a one-dimensional *classical* subspace, the subspace preserving $\alpha = \alpha_*$. The variable v denotes a transverse *nonclassical* dimension used by the noise to construct manifestly nonclassical states. A vivid picture of these states, and their dependence on the noise strength g and pump λ , can now be drawn.

With $\alpha = x$ and $\alpha_* = y$ both real, the Fokker-Planck equation corresponding to Eqs. (2) can be solved in the

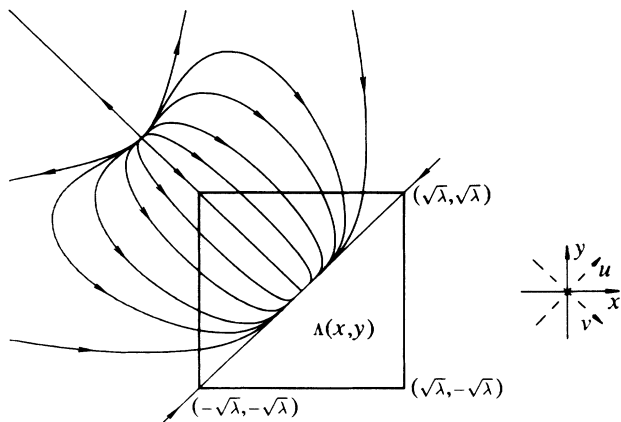


FIG. 1. Deterministic flow on the bounded manifold $\Lambda(x, y)$ for $\lambda = 0.5$. The flow is symmetric about both diagonals through $\Lambda(x, y)$. The origin for the axes shown to the right is located at the center of $\Lambda(x, y)$.

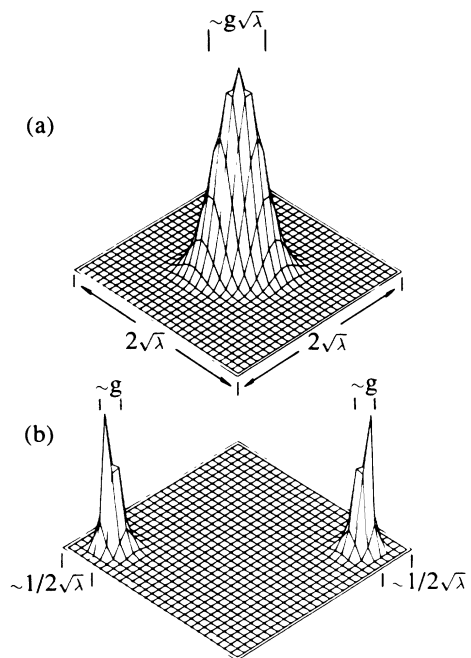


FIG. 2. $P_{ss}(x, y)$ plotted over the manifold $\Lambda(x, y)$ for $g = 0.2$: (a) $\lambda = 0.5$, (b) $\lambda = 2$. $\Lambda(x, y)$ is oriented with the corner $(\sqrt{\lambda}, -\sqrt{\lambda})$ to the front (Fig. 1). Peak widths are labeled for $g \ll 1$, showing that probability is concentrated well away from the boundary of $\Lambda(x, y)$.

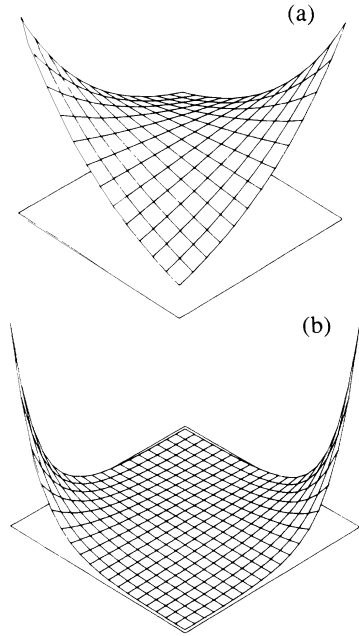


FIG. 3. $P_{ss}(x,y)$ plotted over the manifold $\Lambda(x,y)$ for $g=1$: (a) $\lambda=0.5$, (b) $\lambda=2$. The orientation is the same as Fig. 2.

steady state to obtain ($|x|, |y| \leq \sqrt{\lambda}$)

$$P_{ss}(x,y) = \mathcal{N}[(\lambda - x^2)(\lambda - y^2)]^{1/g^2 - 1} e^{2xy/g^2}, \quad (4)$$

with \mathcal{N} determined by normalization. The steady-state moments derived from Eqs. (3) and (4) agree with those obtained by Drummond, McNeil, and Walls using the complex- P representation.⁵ The advantage of our present formulation is that $P_{ss}(x,y)$ can be plotted, and the classical and nonclassical character of the state discerned in the result.

For weak noise ($g \ll 1$) $P_{ss}(x,y)$ is illustrated in Fig. 2. It strictly vanishes on the boundary of $\Lambda(x,y)$, but is essentially zero well before the boundary is reached. $P_{ss}(x,y)$ is a slightly broadened version of the classical steady states. The picture is precisely that derived from a linearized treatment of the quantum fluctuations. Specifically, with $g \ll 1$ and $\lambda < 1$,

$$P_{ss}(u,v) = \frac{(1-\lambda^2)^{1/2}}{\pi\lambda g/2} \exp\left[-\frac{(1-\lambda)u^2 + (1+\lambda)v^2}{\lambda g^2/2}\right].$$

Recent experiments generating squeezed states belong to this weak-noise regime (in Ref. 1, $g \approx 10^{-4}$). The variances $g^{-2}\langle\Delta u^2\rangle$ and $-g^{-2}\langle\Delta v^2\rangle$ correspond, via Eq. (3), to the normally ordered variances of the unsqueezed and squeezed quadratures, respectively, of the subhar-

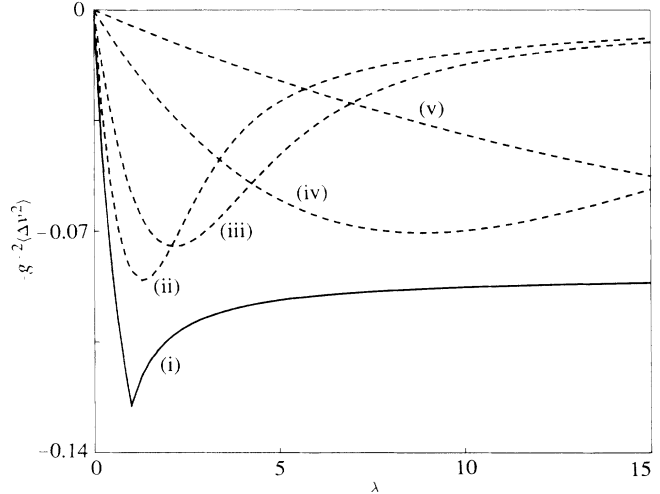


FIG. 4. Intracavity squeezing for (i) $g \ll 1$, (ii) $g=1$, (iii) $g=2$, (iv) $g=5$, and (v) $g=10$.

monic field. Thus, a nonzero variance for the nonclassical variable v is necessary for squeezing. If we keep $g \ll 1$, and set $\lambda=1$, Eq. (4) gives the threshold distribution

$$P_{ss}(u,v) = [4/\sqrt{\pi}g^{3/2}\Gamma(\frac{1}{4})]e^{-(u^4+4v^2)/g^2}.$$

It follows that the threshold photon number (n_{thr}) in the subharmonic mode is $g^{-1}\Gamma(\frac{3}{4})/\Gamma(\frac{1}{4}) \approx 1/3g$; weak noise ($g \ll 1$) corresponds to a large threshold photon number.

Figure 3 shows $P_{ss}(x,y)$ for the same values of λ as Fig. 2, but for $g=1$ rather than $g \ll 1$. The quantum noise has become sufficiently strong to explore thoroughly the nonclassical dimension of the phase space. $P_{ss}(x,y)$ is strongly influenced by the boundary of $\Lambda(x,y)$. The noise strength $g=1$ demarks a qualitative change in the form of $P_{ss}(x,y)$. For $g < 1$, $P_{ss}(x,y)$ strictly vanishes on the boundary, and for $g > 1$ it diverges on the boundary; for $g=1$, $P_{ss}(x,y)$ is nonzero and finite on the boundary.

In the passage to noise strengths $g \geq 1$, the picture built around classical steady states is dramatically altered. The characteristic threshold behavior of the parametric oscillator disappears and squeezing is significantly reduced. This is illustrated by Fig. 4. The departure from the classical picture is most dramatic in the large- g limit. Very strong noise quickly drives all stochastic trajectories to the boundary of $\Lambda(x,y)$, and then along this boundary to the corners, where both noise terms in Eqs. (2) vanish. $P_{ss}(x,y)$ approaches a sum of δ functions:

$$P_{ss}(x,y) = \frac{1}{2} (1 + e^{4\lambda/g^2})^{-1} [\delta(x - \sqrt{\lambda})\delta(y - \sqrt{\lambda}) + \delta(x + \sqrt{\lambda})\delta(y + \sqrt{\lambda})] \\ + \frac{1}{2} (1 + e^{-4\lambda/g^2})^{-1} [\delta(x - \sqrt{\lambda})\delta(y + \sqrt{\lambda}) + \delta(x + \sqrt{\lambda})\delta(y - \sqrt{\lambda})].$$

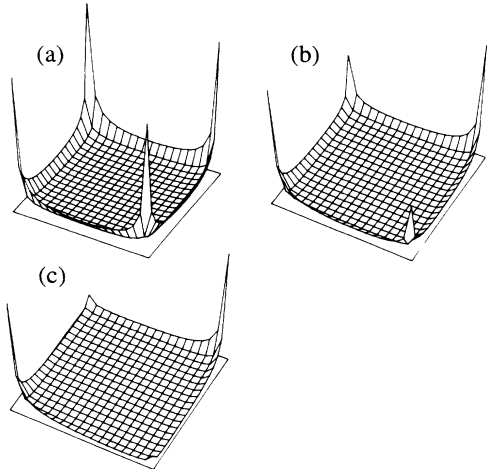


FIG. 5. $P_{ss}(x, y)$ plotted over the manifold $\Lambda(x, y)$ for $g=5$: (a) $\lambda=1$, (b) $\lambda=5$, and (c) $\lambda=15$. The orientation is the same as Fig. 2.

The two δ functions that set $x=y=\pm\sqrt{\lambda}$ represent diagonal terms $|\sqrt{\lambda}/g\rangle\langle\sqrt{\lambda}/g|$ and $|\sqrt{\lambda}/g\rangle\langle-\sqrt{\lambda}/g|$ in the density operator for the subharmonic mode. The two δ functions that set $x=-y=\pm\sqrt{\lambda}$ represent off-diagonal, or interference, terms $e^{2\sqrt{\lambda}/g}|\sqrt{\lambda}/g\rangle\langle-\sqrt{\lambda}/g|$ and $e^{-2\sqrt{\lambda}/g}|\sqrt{\lambda}/g\rangle\langle-\sqrt{\lambda}/g|$.

Figure 5 illustrates the behavior of $P_{ss}(x, y)$ as a function of λ in the strong-noise limit. When $4\lambda/g^2 \ll 1$, all δ functions carry equal weight and the state of the subharmonic field is the *coherent state superposition* $\frac{1}{2}(|\sqrt{\lambda}/g\rangle + |-\sqrt{\lambda}/g\rangle)$. As λ increases, this superposition state is replaced by a *classical mixture* of coherent states $|\sqrt{\lambda}/g\rangle$ and $|\sqrt{\lambda}/g\rangle$ for $4\lambda/g^2 \gg 1$. The disappearance of the interference terms is a consequence of competition between the creation of quantum coherence by the two-mode interaction Hamiltonian and the destruction of this coherence by dissipation. It is known that the decay of quantum coherence for a damped harmonic oscillator prepared in a superposition of coherent states occurs at a rate depending on the phase-space separation of the states.⁶ The separation $2\sqrt{\lambda}/g$ of the coherent states $|\sqrt{\lambda}/g\rangle$ and $|\sqrt{\lambda}/g\rangle$ increases with λ . Eventually, the rate of destruction of quantum coherence by dissipation exceeds the rate of creation of quantum coherence by the two-mode interaction.

What does it mean experimentally to achieve $g \approx 1$? With the nonlinear optical coefficient for $\text{Ba}_2\text{NaNb}_5\text{O}_{15}$, a crystal length of 1 cm, and a beam waist of $1.5 \mu\text{m}$, $g \approx 1$ requires a cavity finesse of 40×10^3 . This can be achieved for mirror transmission losses; but normal crystal losses are 2 orders of magnitude too large. If crystal losses are to be accommodated, an increase of 2 orders of magnitude in the nonlinear optical coefficient is required. An experiment does not seem possible, then, with current materials. However, we emphasize the *general* message of our paper. The parametric oscillator provides an example in which the transition from nearly classical to manifestly quantum-mechanical behavior in a nonlinear quantum dissipative system can be clearly visualized. A similar transition also occurs in other systems. The laser and optical bistability provide good examples. Although we do not have an equally appealing presentation of theory for these examples, experiments on these atomic systems can certainly be designed to access the strong quantum-noise limit.

Through the example of the degenerate parametric oscillator, we have shown that the inclusion of quantum fluctuations in nonlinear dissipative systems is not simply a matter of adding noise to the nonlinear equations of a semiclassical theory. Quantum dissipative systems can exhibit manifestly quantum-mechanical states in the limit of large quantum noise. Traditional thinking about these systems is limited to small noise, where classical states are only slightly perturbed.

This paper is based upon work by the National Science Foundation under Grant No. PHY-84-18070.

¹L. Wu, H. J. Kimble, J. L. Hall, and H. Wu, Phys. Rev. Lett. **57**, 2520 (1986).

²P. Grangier, R. E. Slusher, B. Yurke, and A. LaPorta, Phys. Rev. Lett. **59**, 2153 (1987).

³H. J. Carmichael, J. S. Satchell, and S. Sarkar, Phys. Rev. A **34**, 3166 (1986).

⁴H. J. Carmichael and M. Wolinsky, in *Quantum Optics IV*, edited by J. D. Harvey and D. F. Walls (Springer-Verlag, Berlin, 1986), pp. 208–220.

⁵P. D. Drummond, K. J. McNeil, and D. F. Walls, Opt. Acta **28**, 211 (1980).

⁶A. O. Caldeira and A. J. Leggett, Phys. Rev. A **31**, 1059 (1985).